Supporting Information

Amorphous cobalt phosphate incorporated in carbon matrix as an efficient pre-catalyst for promoted electrosynthesis of ammonia

Fengcai Lei,[†,*,a] Mengmeng Xu,[†,a] Yiming Zhang,[a] Jing Yu,[a] Menghan Zhang,[a] Ruixue Huai,[a] Junfeng Xie,[a] Pin Hao,[a] Guanwei Cui[a] and Bo Tang*[,a,b]

[a.] College of Chemistry, Chemical Engineering and Materials Science, Key Laboratory of Molecular and Nano Probes (Ministry of Education), Collaborative Innovation Center of Functionalized Probes for Chemical Imaging in Universities of Shandong, Institute of Molecular and Nano Science, Shandong Normal University, Jinan, Shandong, 250014, P. R. China. E-mail: leifc@sdnu.edu.cn; tangb@sdnu.edu.cn

[b.] Laoshan Laboratory, Qingdao 266237, Shandong, P. R. China.

† These authors contributed equally.

Experimental details

Chemicals

Cobalt nitrate hexahydrate ($Co(NO_3)_2 \cdot 6H_2O$, > 99%), Sodium hypophosphite monohydrate ($NaH_2PO_2 \cdot H_2O$, > 99%), N-(1-naphthyl) ethylenediamine dihydrochloride and 2-methylimidazole ($C_4H_6N_2$, > 98%) were purchased from Aladdin Chemical reagent Co., Ltd. (Shanghai, China). Nafion solution (5 wt%) and $K^{15}NO_3$ (99 atom%; ≧99.0%) were purchased from Sigma-Aldrich. Potassium hydroxide (KOH), potassium nitrate (KNO_3), sodium hydroxide (NaOH), and other reagents related to determination of ion concentration (salicylic acid, sodium nitroprusside dihydrate, sodium hypochlorite aqueous solution, ammonium chloride, sodium nitrate, phosphoric acid, sodium citrate and p-aminobenzene sulfonamide) were purchased from Sinopharm Chemical Reagent Co., Ltd. All the chemicals were used directly without further purification.

Experimental section

Synthesis of ZIF-67 crystals

Two solutions were prepared by dissolving 2-methylimidazole and $Co(NO_3)_2 \cdot 6H_2O$ in 50 mL of methanol, respectively. Then, they were mixed together. The resulted solution was stirred for 24 hours at room temperature. The resulted precipitates can collect by centrifugation, and then washed by methanol four times, finally vacuum-dried at 40℃.

Synthesis of the Co-P-O/C

The obtained ZIF-67 was put into a porcelain boat with NaH_2PO_2 (weight ratios 1:10) at the upstream side of the furnace. Subsequently, the powder was annealed at 300°C with a ramping rate of 2 °C·min^{-1} and kept for 2 h in N_2 flow, and then cooled to ambient temperature under N_2 to obtain Co-P-O/C-2. Co-P-O/C-1 and Co-P-O/C-3 were prepared by the same procedure except for the weight ratios set as 1:5 and 1:20, respectively.

Synthesis of the ZIF-67-300

To prepare ZIF-67-300, the NIF-67 was annealed at 300°C for 2 h at a ramping rate of 2 °C·min^{-1} under the protection of N_2.

Electrochemical measurements

The electrochemical measurement was tested on electrochemical workstation (CHI660E, Shanghai Chenhua) with using a three-electrode H-type electrolytic cell assembled by Nafion

membrane. The working electrode was prepared as follows: 5 mg of prepared catalyst and 40 μL Nafion solution (Sigma Aldrich, 5 wt%) were dispersed in 1 mL ethanol and water mixed solution by sonicating for at least 30 min to form a homogeneous ink. Then 5 μL of the dispersion (containing 24 μg of catalyst) was loaded onto a glassy carbon electrode with 3 mm diameter. The platinum gauze and the Hg/HgO electrode were used as counter electrode and reference electrode, respectively. All the potentials were recorded to reversible hydrogen electrode (RHE) by the Nernst equation. For nitrate reduction, the linear sweep voltammetry (LSV) was carried out in Ar saturated 1 M KOH solution with 0.1 M KNO_3 contained. Then the potentiostatic tests were tested to quantify the nitrate performance at every 0.1 V from −0.1 V to −0.6 V. The electrochemical impedance spectroscopy (EIS) measurements were operated at −0.2 V from 1-10^5 Hz. Cyclic voltammetry (CV) was performed at various scan rates (20, 40, 60,80, 100 mV s^{-1}) in region of 0.2 ~0.3 V. The electrochemical double-layer capacitance (C_{dl}) of various samples can be determined from the cyclic voltammograms. The C_{dl} was estimated by plotting the Δj (j_{anode}-$j_{cathode}$) at 0.25 V vs RHE against the scan rate, where the slope is twice C_{dl}.

Characterization

X-ray diffraction (XRD) was performed on a Philips X'Pert Pro Super diffractometer with Cu Kα radiation (λ = 1.54178 Å). The scanning electron microscopy (SEM) images were taken on a JEOL JSM-6700F SEM. The transmission electron microscopy (TEM) was carried out on a JEM-2100F field emission electron microscope at an acceleration voltage of 200 kV. X-ray photoelectron spectroscopy (XPS) analyses were performed on a VGESCALAB MKII X-ray photoelectron spectrometer with an excitation source of Mg Kα = 1253.6 eV, and the resolution level was lower than 1 atom%. Raman spectra were performed on a LabRAM HR Evolution Raman spectrometer, the laser excitation was 532 nm, and the exposure time was 2 s. The ultraviolet-visible (UV-Vis) absorbance spectra were measured on UV-Vis Spectrophotometer (Shimadzu UV-2600). The isotope labeling experiments were measured by ^{1}H-NMR measurement (Bruker 600 MHz system).

Determination of ion concentration

The products in the electrolytes before and after electrochemical process were detected by the UV-Vis spectrophotometer. The detailed methods are as follows:

Determination of nitrite:

P-aminobenzene sulfonamide (4 g), N-(1-naphthyl) ethylenediamine dihydrochloride (0.2 g), phosphoric acid (10 mL, ρ=1.70 g mL^{-1}) were mixed and diluted to 100 mL with ultrapure water for using as a color reagent. A certain amount of electrolyte was taken out from the electrolytic cell and diluted to the detection range. Next, 1 mL of the above diluted solution was mixed with 0.1 mL of color reagent uniformity, and the absorption intensity at the wavelength of 540 nm was recorded after sitting for 20 minutes. The concentration-absorbance curve was calibrated using a series of standard sodium nitrite solutions.

Determination of ammonia:

Ammonia was quantified by the indophenol blue method. After the catalysis was completed, a certain amount of electrolyte was taken out from the electrolytic cell and diluted to the detection range to ensure that the ammonia concentrations in the test solution were within the linear range of the indole blue method. The color reagent was composed of 50 g L^{-1} salicylic acid solution, 10 g L^{-1} sodium nitroprusside dihydrate solution and 0.05 mol L^{-1} sodium hypochlorite solution. 1 mL of the diluted electrolyte was mixed with 0.5 mL of salicylic acid solution, 0.1 mL of sodium nitroprusside dihydrate solution and 0.1 mL of sodium hypochlorite solution. The absorption intensity at the wavelength of 660 nm was recorded after sitting for 1 h. The concentration-absorbance curve was calibrated using a series of standard ammonium chloride solutions.

The specific solution preparation method are as follows:

Salicylic acid solution (50 g L^{-1}): 10 g salicylic acid, 10 g sodium citrate and 55 mL sodium hydroxide solution [c(NaOH)= 2 mol L^{-1}] were added into 50 mL water, then the solution was diluted with ultrapure water to 200 mL. It was stable for one month at room temperature.

Sodium nitroprusside dihydrate solution (10 g L^{-1}): 1 g of sodium nitroprusside dihydrate was dissolved in 100 mL of ultrapure water.

Calculation of ammonia yield, and Faradaic efficiency

The calculation of ammonia yield uses the following equation:

$$Yield(NH_3) = (C \times V)/(m \times t)$$

where C is the concentration of NH_3 (aq), V is the volume of the electrolyte, m is the mass of loaded catalyst and t is the reaction time.

The calculation of Faraday efficiency uses the following equation:

$$Faradaic\ efficiency = [(C \times V \times F \times n)/Q] \times 100\%$$

where C is the concentration of NH_3 (aq) or NO_2^- (aq) in the electrolyte, V is the volume of the electrolyte, n is the number of electrons transferred (For NH_3, n=8; for NO_2^-, n=2), F is the Faraday constant (96485 C mol^{-1}), and Q is the total charge passing the electrode.

^{15}N isotope labeling experiment

The isotopic labeling nitrate reduction experiments were carried out using the above electrochemical nitrate reduction methods, except the N-source was replaced by $K^{15}NO_3$ (99 atom%; ≥99.0%). After performing potentiostatic electrolysis, the pH of the electrolyte was acidified to 2 ~ 3 with the HCl solution. Then, DMSO (dimethyl sulfoxide) was mixed with the acidified electrolyte. $^{15}NH_4^+$ was detected by ^{1}H NMR measurement. (^{1}H NMR, Bruker 600 MHz). $^{14}NH_4^+$ was also detected by ^{1}H NMR by the same method except for the N-source was $K^{14}NO_3$. For the quantitative analysis of ammonia, maleic acid was used as internal standards.

In situ Raman spectroscopy measurements

Raman spectra were collected via the Horiba HR Evolution Raman microscope system. We conducted the electrochemical experiments on a homemade Raman spectro-electrochemical cell with 1 M KOH and 0.1 M KNO_3 contained. During the measurement, the long-focus objective of 50× was adopted, and the laser power was set as 4.8 mW with wavelength of 532 nm. The diffraction grid was 600 gr/mm, and integration time was set as 2 s.

Supplementary Figures

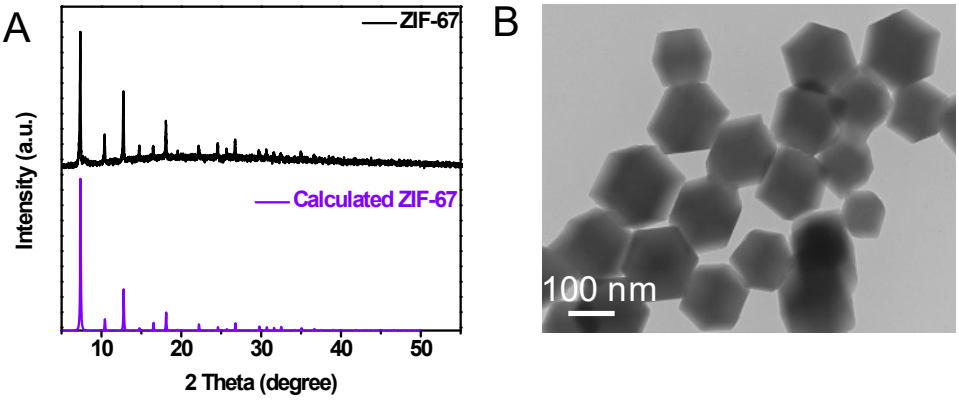

Fig. S1. (A) XRD patterns of ZIF-67; (B) TEM image of ZIF-67.

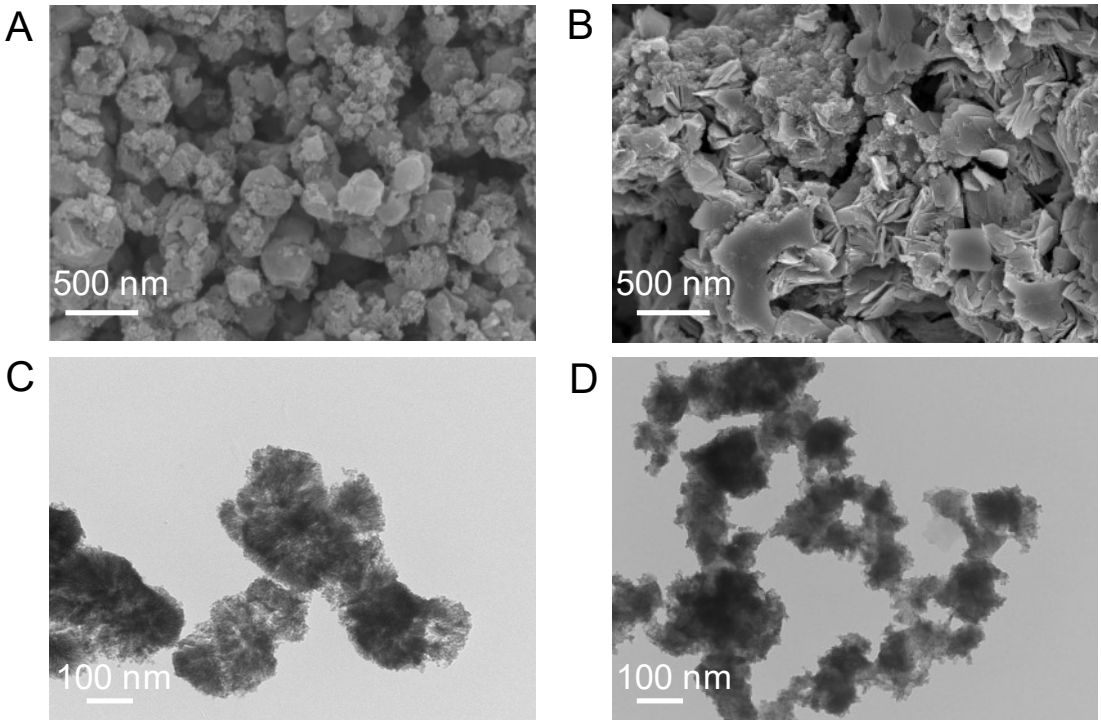

Fig. S2. SEM images of (A) Co-P-O/C-1 and (B) Co-P-O/C-3; TEM images of (C) Co-P-O/C-1 and (D) Co-P-O/C-3.

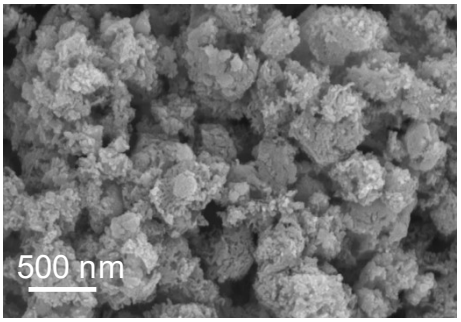

Fig. S3. SEM image of Co-P-O/C-2. Compared with Co-P-O/C-1, less characteristics of ZIF-67 can be observed, indicating higher degree of phosphorization of Co-P-O/C-2.

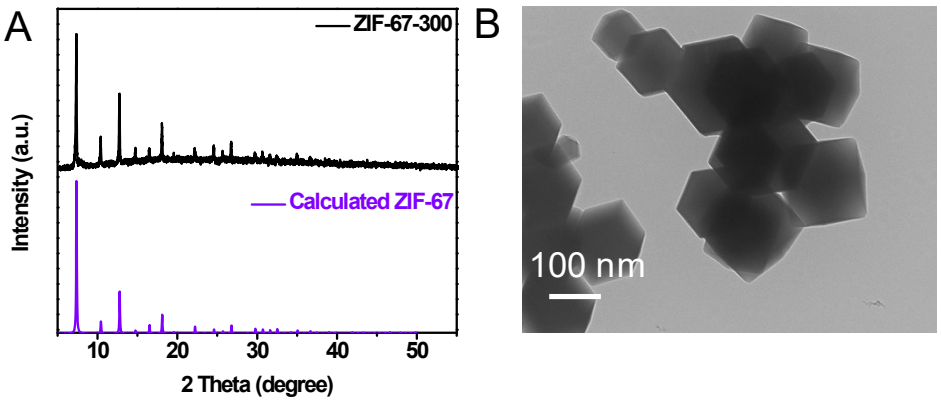

Fig. S4. (A) XRD patterns of ZIF-67-300; (B) TEM image of ZIF-67-300.

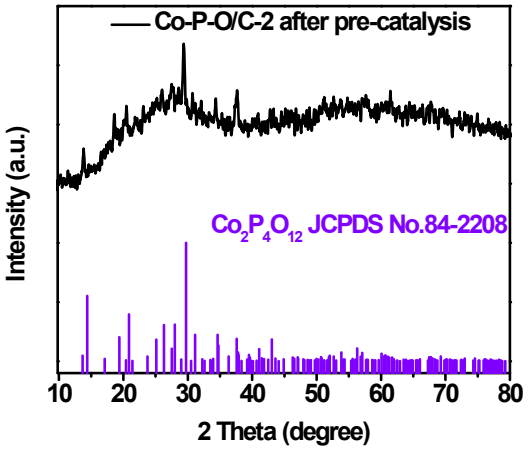

Fig. S5. XRD pattern of Co-P-O/C-2 after pre-catalytic process.

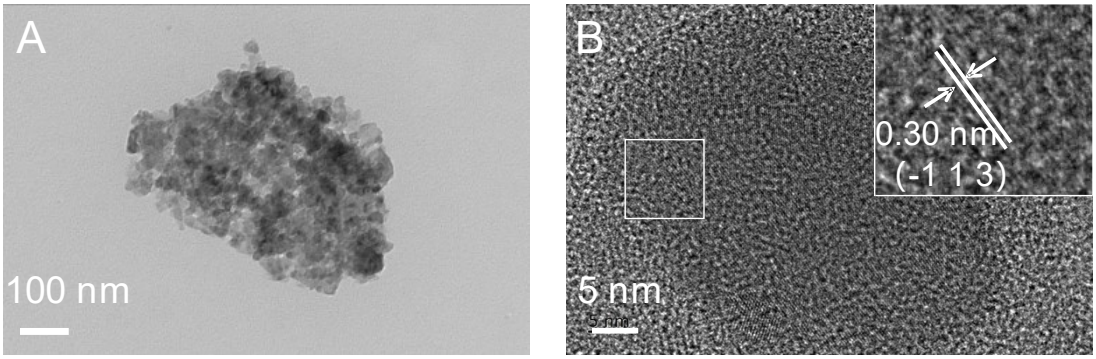

Fig.S6. Characterizations of Co-P-O/C-2 after long-term electrochemical test: (A) TEM image; (B) HRTEM image.

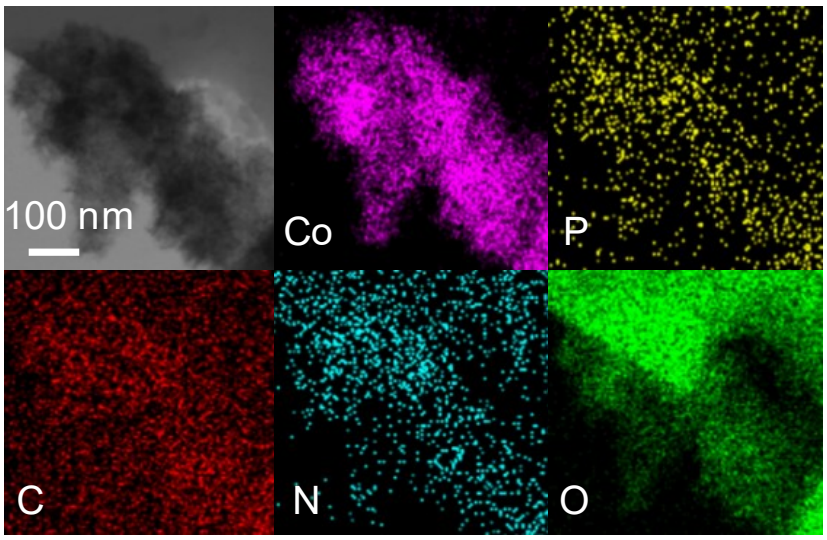

Fig. S7. EDS elemental mapping of the Co-P-O/C-2 after electrochemical test，including Co, P, C, N, and O.

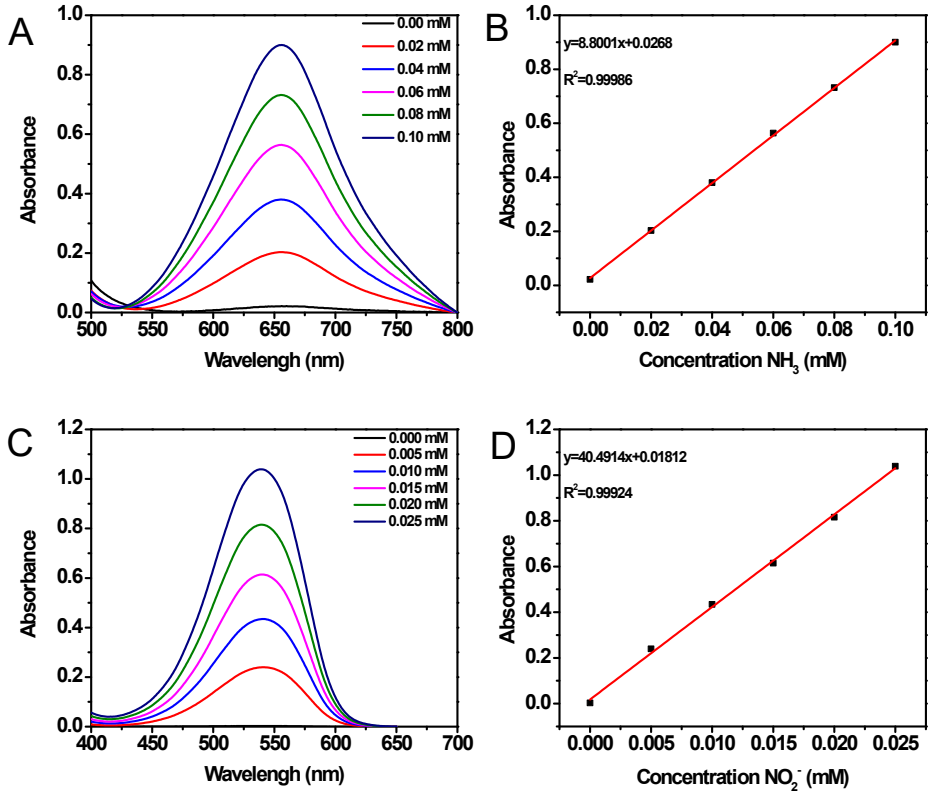

Fig. S8. Plotting of standard curves of (A, B) ammonia, (C, D) nitrite in 1 M KOH solution.

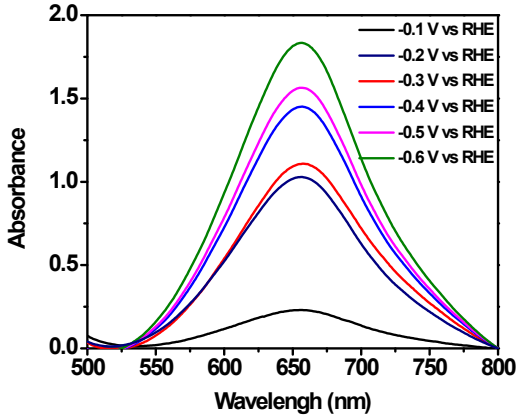

Fig. S9. UV-Vis absorption spectra of ammonia in nitrate reduction performances of Co-P-O/C-2 at different applied potentials.

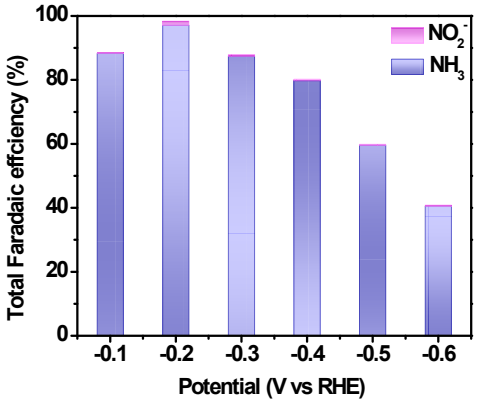

Fig. S10. Nitrate reduction performance of Co-P-O/C-2: Faradaic efficiency of ammonia and nitrite at different potentials in 1 M KOH with 0.1 M KNO_3.

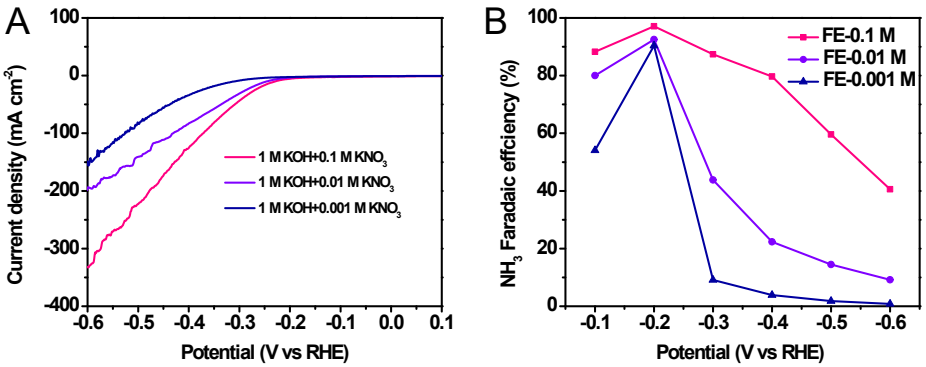

Fig. S11. (A) LSV curves of Co-P-O/C-2 in 1.0 M KOH with different NO_3^- concentrations. (B) FE of NH_3 tested at different potentials of Co-P-O/C-2 at each applied potential. According to the LSV curves of different nitrate concentrations in 1 M KOH, the current densities decrease with lower concentration of NO_3^-. Importantly, the catalyst exhibits nearly the same FE trajectory

when the nitrate concentration varied from 0.001 M to 0.1 M. It can reach the highest FE of 90% even at the low concentration of 0.001 M, indicating the high selectivity of NH_3 at −0.2 V vs RHE of Co-P-O/C-2. In the more negative potentials, the NH_3 FEs drop rapidly because of activated HER process in the such low concentration of NO_3^-. These results show the catalyst sustainable and energy-efficient prospect in the field of NH_3 synthesis from dilute nitrate solution.

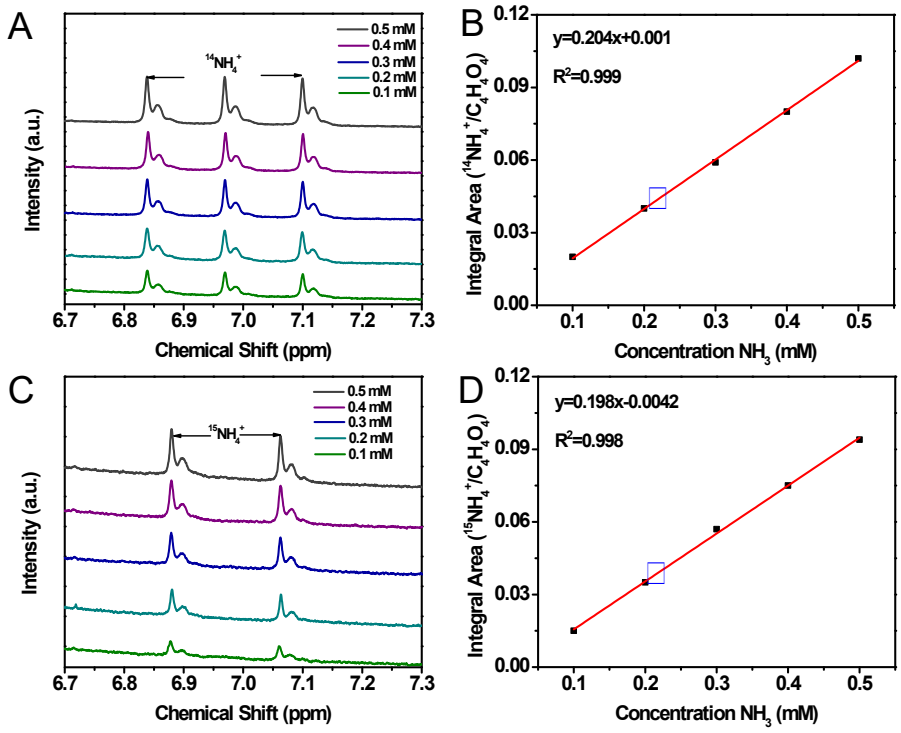

Fig. S12. (A) The ^1H NMR spectra of different $^{14}NH_4^+$ concentrations. (B) The standard curve of integral area ($^{14}NH_4^+/C_4H_4O_4$) against $^{14}NH_4^+$ concentration. (C) The ^1H NMR spectra of different $^{15}NH_4^+$ concentrations. (D) The standard curve of integral area ($^{15}NH_4^+/C_4H_4O_4$) against $^{15}NH_4^+$ concentration. The symbols in B and D are the values in our experiment. The $^{15}NH_3$ synthesized at −0.2 V for 2 h is 2085 mmol g_{cat}^{-1} h^{-1}, which is close to $^{14}NH_3$ tested by ^1H NMR (2090 mmol g_{cat}^{-1} h^{-1}) and indophenol method (2006 mmol g_{cat}^{-1} h^{-1}), suggesting the accuracy of both two detection methods and further confirming that the synthesized ammonia was totally derived from nitrate reduction.

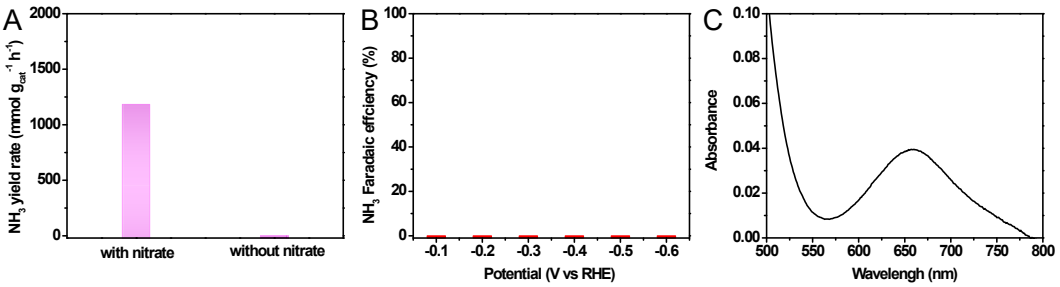

Fig. S13. Performance of Co-P-O/C-2: (A) Ammonia yield rate in electrolyte with or without nitrate at −0.2 V vs RHE; (B) ammonia Faradaic efficiency in pure 1 M KOH, (C) UV-Vis absorption spectra of possible ammonia in KNO_3 before electrocatalytic performance and negligible ammonia can be detected.

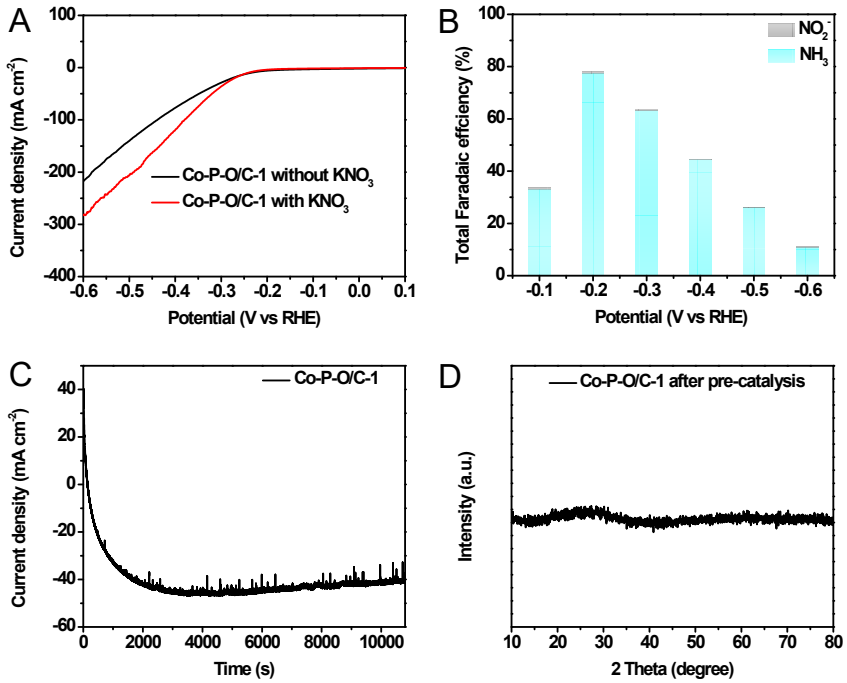

Fig. S14. Nitrate reduction performance of Co-P-O/C-1: (A) LSV curves of Co-P-O/C-1 in 1 M KOH electrolyte with and without nitrate, (B) Faradaic efficiency of ammonia and nitrite at different potentials, (C) i-t curve at −0.2 V vs RHE, (D) XRD pattern of Co-P-O/C-1 after pre-catalytic process.

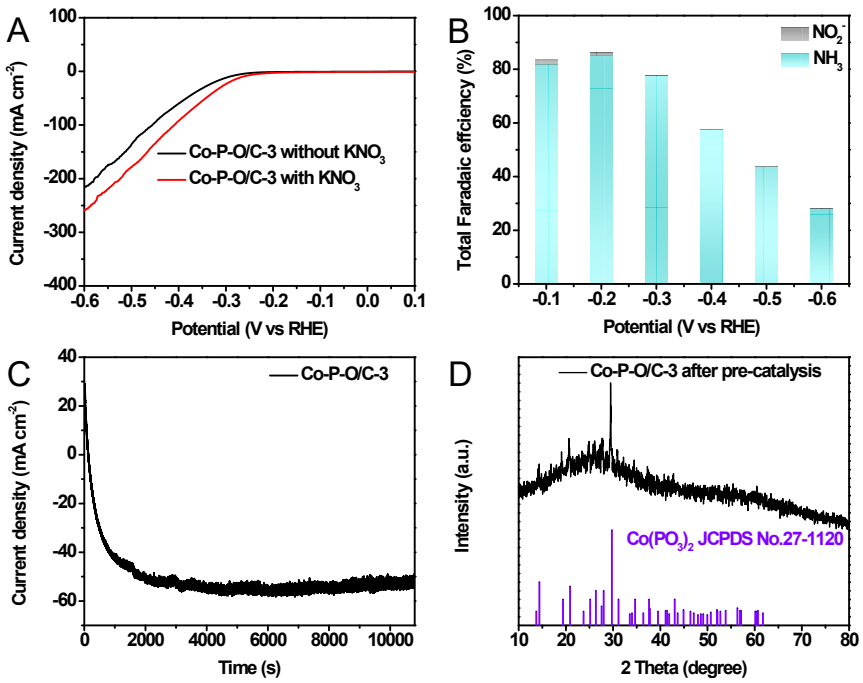

Fig. S15. Nitrate reduction performance of Co-P-O/C-3: (A) LSV curves of Co-P-O/C-3 in 1 M KOH electrolyte with and without nitrate, (B) Faradaic efficiency of ammonia and nitrite at different potentials, (C) i-t curve at −0.2 V vs RHE, (D) XRD pattern of Co-P-O/C-3 after pre-catalytic process.

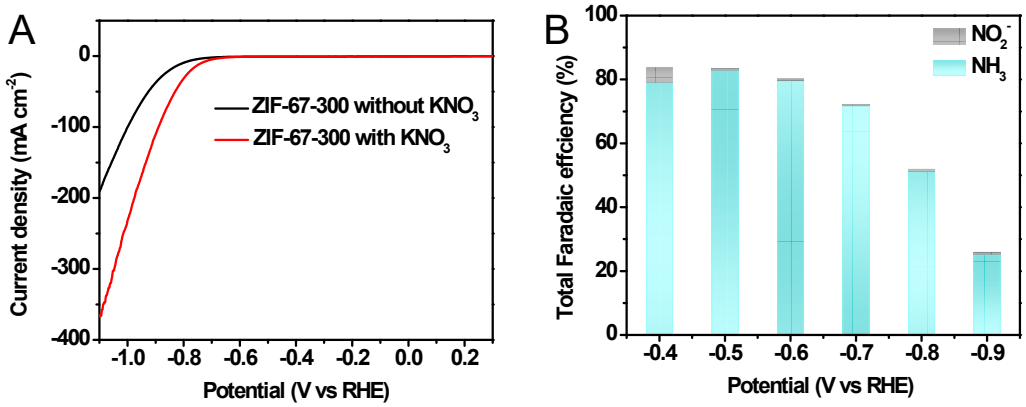

Fig. S16. Nitrate reduction performance of ZIF-67-300: (A) LSV curves of ZIF-67-300 in 1 M KOH electrolyte with and without nitrate, (B) Faradaic efficiency of ammonia and nitrite at different potentials. The FE measured from −0.4 V vs RHE, because the produced ammonia was too low to detect when more positive potentials applied.

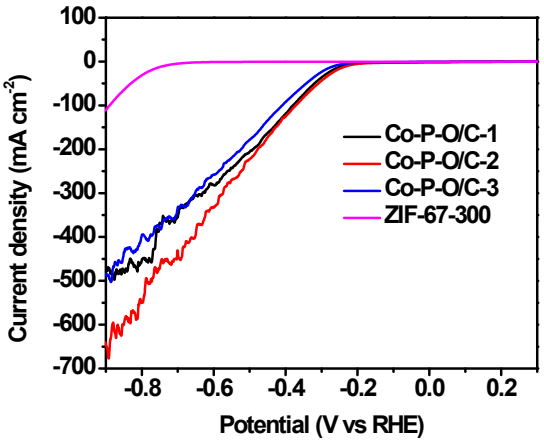

Fig. S17. LSV curves of Co-P-O/C-1, Co-P-O/C-2, Co-P-O/C-3 and ZIF-67-300 in 1 M KOH with 0.1 M KNO_3.

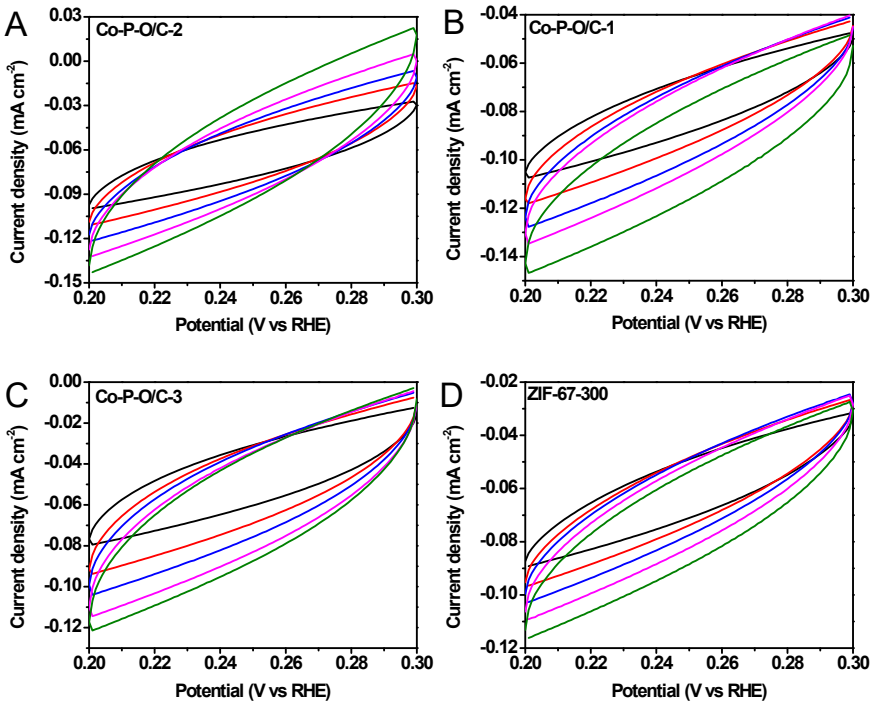

Fig. S18. Cyclic voltammetry curves of (A) Co-P-O/C-2, (B) Co-P-O/C-1, (C) Co-P-O/C-3 and (D) ZIF-67-300 in the region of 0.2~0.3 V vs RHE.

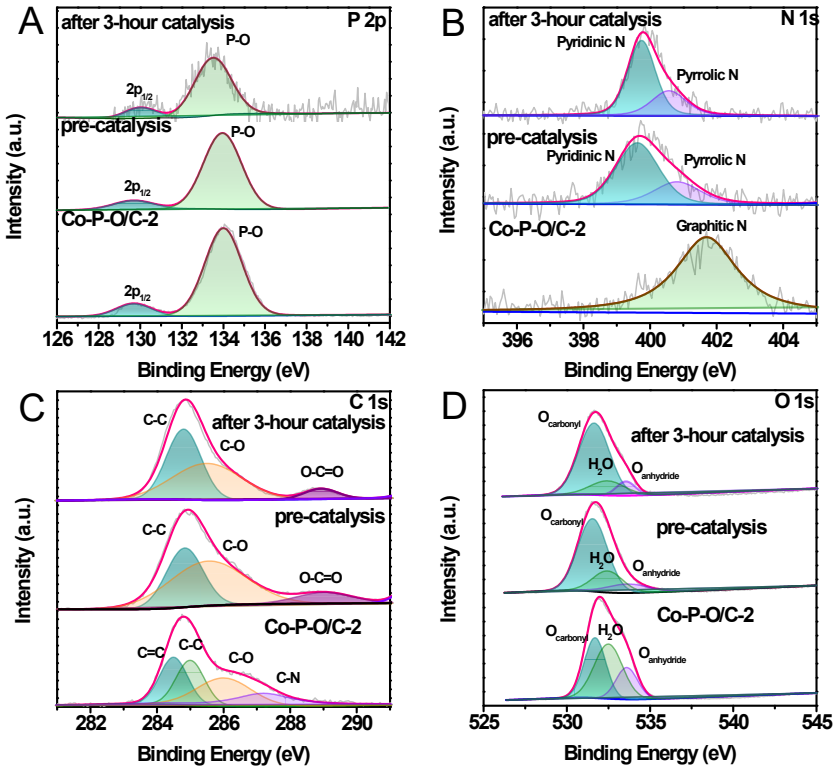

Fig. S19. XPS spectra of (A) P 2p, (B) N 1s, (C) C 1s and (D) O 1s of original Co-P-O/C-2, Co-P-O/C-2 after pre-catalysis and after 3-hour catalysis. After pre-catalysis, diminished metal-P bond can be observed due to the seriously phase transformation.

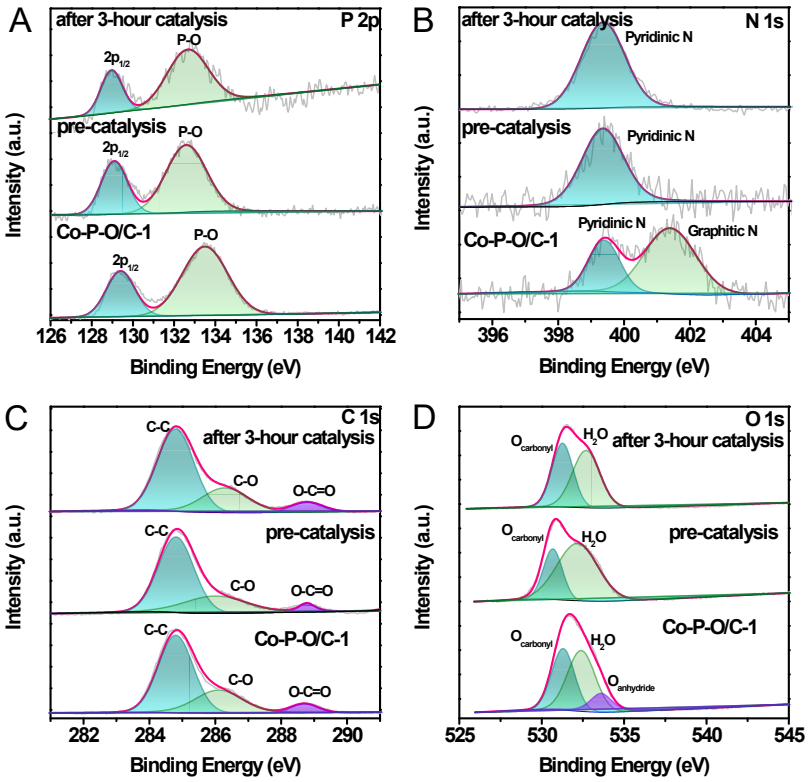

Fig. S20. XPS spectra of (A) P 2p, (B) N 1s, (C) C 1s and (D) O 1s of original Co-P-O/C-1, Co-P-O/C-1 after pre-catalysis and after 3-hour catalysis. The Co-P bond after 3-hour catalysis in P 2p core level is slightly weaker than the original one and obviously stronger than that of Co-P-O/C-2 in Fig. S19A, suggesting the inadequate phase construction of Co-P-O/C-1.

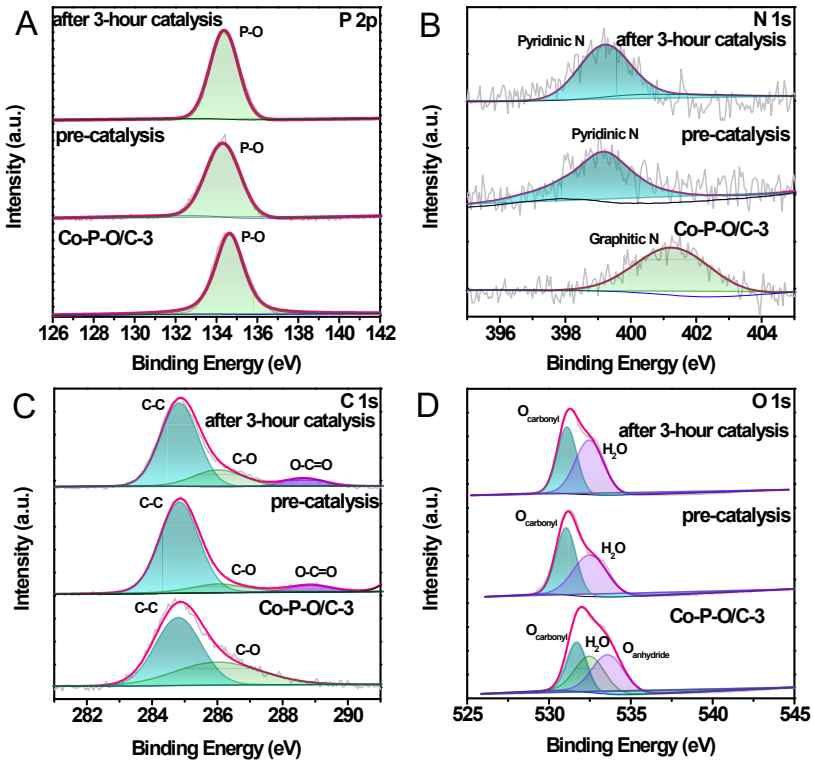

Fig. S21. XPS spectra of (A) P 2p, (B) N 1s, (C) C 1s and (D) O 1s of original Co-P-O/C-3, Co-P-O/C-3 after pre-catalysis and after 3-hour catalysis. No obvious variation can be observed on catalyst of Co-P-O/C-3 after long-term catalytic process.

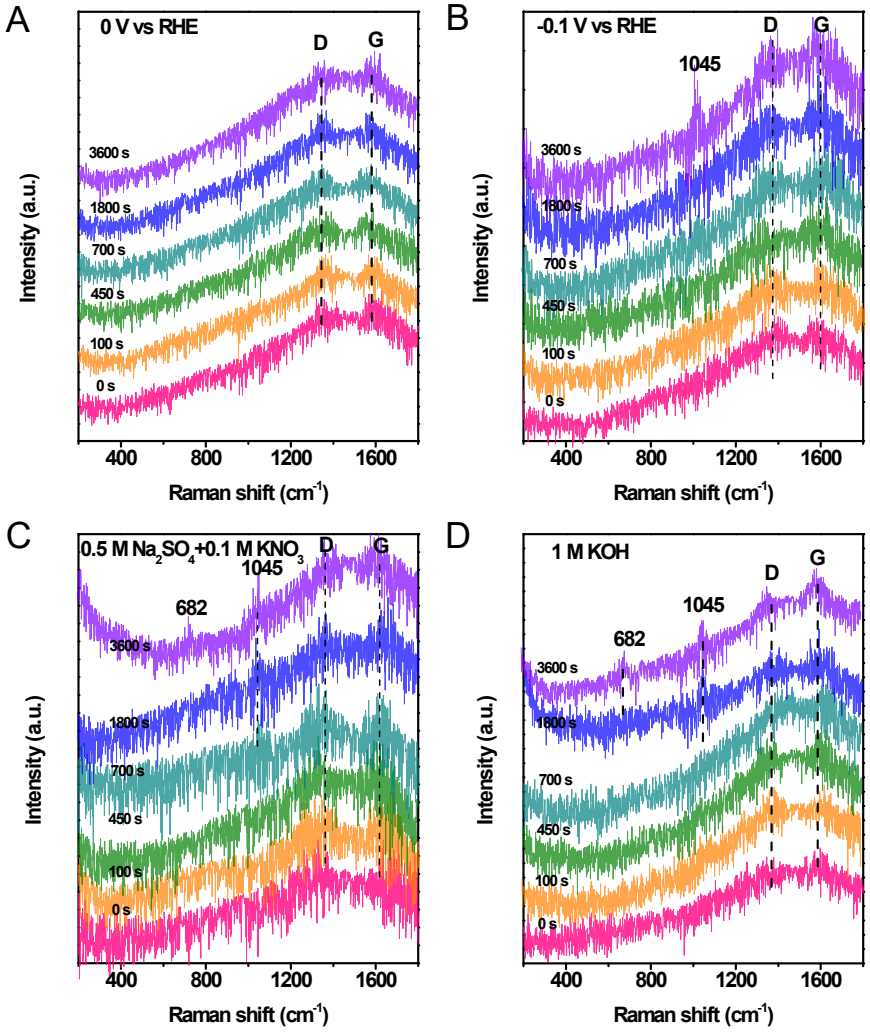

Fig. S22. *In situ* Raman spectra of Co-P-O/C-2 during different catalytic processes: (A, B) with 1 M KOH and 0.1 M KNO_3 at 0 V vs RHE and −0.1 V vs RHE, respectively; (C) with 0.5 M Na_2SO_4 and 0.1 M KNO_3 at −0.2 V vs RHE and (D) with 1 M KOH at −0.2 V vs RHE.

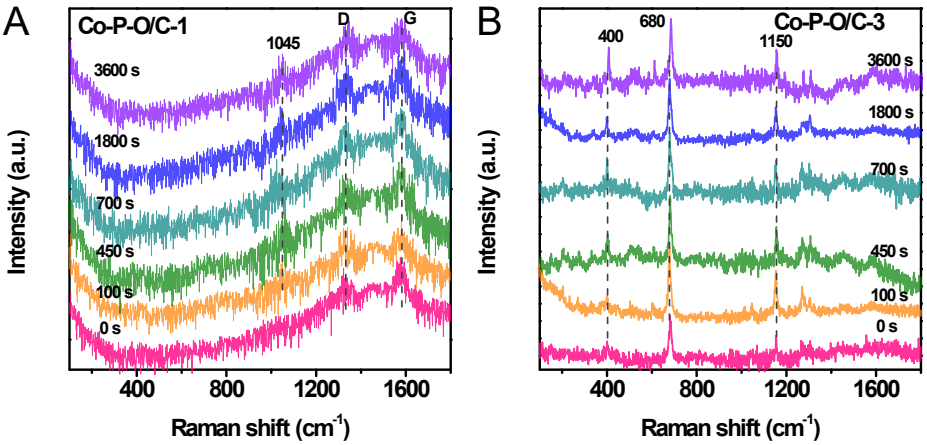

Fig. S23. *In situ* Raman spectra of (A) Co-P-O/C-1 and (B) Co-P-O/C-3 during catalytic process

at −0.2 V vs RHE.

.

Table S1 Comparison of ammonia synthesis activity by Co-P-O/C-2 and other catalysts.

Catalysts	Electroreduction condition	NH_3 Yield rate/Faradaic efficiency	Reference	Potential under optimal ammonia efficiency
Pd/TiO_{2-x}	0.25 M NO_3^-	1.12 mg cm^{-2} h^{-1}/92.05%	[1]	−0.7 V vs RHE
CoP/TiO_2@TP	0.1 M NaOH +0.1 M NO_3^-	499.8 μmol h^{-1} cm^{-2}/95.0%	[2]	−0.3 V vs RHE
Ni_2P/NF	0.1 M PBS+200 ppm NO_3^-	2692.2 μg h^{-1} cm^{-2}/90.2%	[3]	−0.3 V vs RHE
Co-P-O/TP	0.2 M PBS+200 ppm NO_3^-	248.1 μg h^{-1} cm^{-2}/93.3%	[4]	−0.2 V vs RHE
Co_2AlO_4/CC	0.1 M PBS+0.1 M NO_3^-	7.9 mg h^{-1} cm^{-2}/92.6%	[5]	−0.7 V vs RHE
Fe SACs	0.25 M K_2SO_4+0.5 M KNO_3/0.1 M K_2SO_4	0.46 mmol h^{-1} cm^{-2}/75%	[6]	−0.66 V vs RHE
pCuO-5	0.05 M H_2SO_4+0.05 M NO_3^-	--/89%	[7]	−0.5 V vs RHE
Co-Fe@Fe_2O_3	0.1 M Na_2SO_4+500 ppm NO_3^-	880.52 μg h^{-1} cm^{-2} /85.23%	[8]	−0.745 V vs RHE
FTO-E	PBS+0.1 M $NaNO_3$	13.13 mg h^{-1} mg^{-1}_{cat}/87.5%	[9]	−1.0 V vs RHE
TiO_2 nanotubes	50 mg L^{-1} NO_3^-+0.5 M Na_2SO_4	0.045 mmol h^{-1} mg^{-1}_{cat}/85%	[10]	−0.95 V vs RHE

Table S2 The charge transfer resistance (R_{ct}) value of each sample.

Catalyst	R_{ct} (Ω)
Co-P-O/C-1	107.3
Co-P-O/C-2	63.6
Co-P-O/C-3	110.1
ZIF-67-300	5563.3

Reference

[1] Y. Guo, R. Zhang, S. Zhang, Y. Zhao, Q. Yang, Z. Huang, B. Dong, C. Zhi, Pd doping-weakened intermediate adsorption to promote electrocatalytic nitrate reduction on TiO_2 nanoarrays for ammonia production and energy supply with zinc–nitrate batteries, Energy Environ. Sci., 14 (2021) 3938-3944.

[2] Z. Deng, C. Ma, X. Fan, Z. Li, Y. Luo, S. Sun, D. Zheng, Q. Liu, J. Du, Q. Lu, B. Zheng, X. Sun, Construction of CoP/TiO_2 nanoarray for enhanced electrochemical nitrate reduction to ammonia, Mater. Today Phys., 28 (2022) 100854.

[3] G. Wen, J. Liang, L. Zhang, T. Li, Q. Liu, X. An, X. Shi, Y. Liu, S. Gao, A.M. Asiri, Y. Luo, Q. Kong, X. Sun, Ni_2P nanosheet array for high-efficiency electrohydrogenation of nitrite to ammonia at ambient conditions, J. Colloid Interface Sci., 606 (2022) 1055-1063.

[4] Z. Li, G. Wen, J. Liang, T. Li, Y. Luo, Q. Kong, X. Shi, A.M. Asiri, Q. Liu, X. Sun, High-efficiency nitrate electroreduction to ammonia on electrodeposited cobalt-phosphorus alloy film, Chem. Commun., 57 (2021) 9720-9723.

[5] Z. Deng, J. Liang, Q. Liu, C. Ma, L. Xie, L. Yue, Y. Ren, T. Li, Y. Luo, N. Li, B. Tang, A. Ali Alshehri, I. Shakir, P.O. Agboola, S. Yan, B. Zheng, J. Du, Q. Kong, X. Sun, High-efficiency ammonia electrosynthesis on self-supported Co_2AlO_4 nanoarray in neutral media by selective reduction of nitrate, Chem. Eng. J., 435 (2022) 135104.

[6] Z.Y. Wu, M. Karamad, X. Yong, Q. Huang, D.A. Cullen, P. Zhu, C. Xia, Q. Xiao, M. Shakouri, F.Y. Chen, J.Y.T. Kim, Y. Xia, K. Heck, Y. Hu, M.S. Wong, Q. Li, I. Gates, S. Siahrostami, H. Wang, Electrochemical ammonia synthesis via nitrate reduction on Fe single atom catalyst, Nat. Commun., 12 (2021) 2870.

[7] R. Daiyan, T. Tran-Phu, P. Kumar, K. Iputera, Z. Tong, J. Leverett, M.H.A. Khan, A. Asghar Esmailpour, A. Jalili, M. Lim, A. Tricoli, R.-S. Liu, X. Lu, E. Lovell, R. Amal, Nitrate reduction to ammonium: from CuO defect engineering to waste NO_x-to-NH_3 economic feasibility, Energy Environ. Sci., 14 (2021) 3588-3598.

[8] S. Zhang, M. Li, J. Li, Q. Song, X. Liu, High-ammonia selective metal-organic framework-derived Co-doped Fe/Fe_2O_3 catalysts for electrochemical nitrate reduction, Proc. Natl. Acad. Sci. U. S. A., 119 (2022) e2115504119.

[9] H. Du, H. Guo, K. Wang, X. Du, B.A. Beshiwork, S. Sun, Y. Luo, Q. Liu, T. Li, X. Sun, Durable Electrocatalytic Reduction of Nitrate to Ammonia over Defective Pseudobrookite Fe_2TiO_5 Nanofibers with Abundant Oxygen Vacancies, Angew. Chem. Int. Ed., 62 (2023) e202215782.

[10] R. Jia, Y. Wang, C. Wang, Y. Ling, Y. Yu, B. Zhang, Boosting Selective Nitrate Electroreduction to Ammonium by Constructing Oxygen Vacancies in TiO_2, ACS Catal., 10 (2020) 3533-3540.